C. R. Physique 11 (2010) 68–76

Contents lists available at ScienceDirect

Comptes Rendus Physique

Propagation and remote sensing / Propagation et télédétection

Monostatic Radar Cross Section of an object above a sea surface from a rigorous method

Surface Equivalente Radar monostatique d'un objet au-dessus de la mer par une méthode rigoureuse

Gildas Kubické *, Christophe Bourlier, Joseph Saillard

IREENA, Fédération CNRS Atlanstic, Université Nantes Angers Le Mans, Polytech'Nantes, La Chantrerie, BP 50609, 44306 Nantes, France

ARTICLE INFO

Article history:
Available online 20 February 2010

Keywords:
Object detection
Remote sensing
Monostatic RCS
Fast numerical method

Mots-clés :
Détection d'objet
Domaine maritime
SER monostatique
Méthode numérique rapide

ABSTRACT

The rigorous computation of the monostatic RCS (Radar Cross Section) of an object above a one-dimensional sea surface (2D case) needs to solve a problem involving a high number of unknowns. Thus, a recently developed fast numerical method, called E-PILE (Extended Propagation-Inside-Layer Expansion), was combined with FB-SA (Forward–Backward with Spectral Acceleration). Two objects are considered in this article: the cross and the cylinder. Results obtained from E-PILE + FB-SA allow us to understand the physical mechanisms involved in the coupling between the object and the sea surface.

RÉSUMÉ

Le calcul rigoureux de la SER (Surface Equivalente Radar) monostatique d'un objet situé au-dessus d'une surface de mer monodimensionnelle (cas 2D) nécessite de résoudre un problème possédant un grand nombre d'inconnues. Pour ce calcul, une méthode numérique rapide récemment développée, nommée E-PILE (Extended Propagation-Inside-Layer Expansion), est combinée à la FB-SA (Forward–Backward with Spectral Acceleration). Deux objets sont considérés dans ce papier: l'obstacle cruciforme (la croix) et le cylindre. L'étude des résultats issus de la méthode E-PILE + FB-SA permet de bien comprendre les mécanismes physiques du couplage de l'obstacle et de la surface de mer. L'application visée est la détection d'obstacles pour la télédétection en milieu maritime.

1. Introduction

The study of scattering from an object above a rough surface is a subject of great interest. The applications of such research concern many areas such as remote sensing, radar surveillance, optics and acoustics. Since the sea surface can be modeled as a rough surface, these applications are useful for maritime domain in which some radar reflectors are used in several situations: mounted on a buoy to mark a shoal or mounted on a ship's mast, for example. Such a problem implies many parameters, such as incidence angle, frequency, shape and size of the reflector, position above the surface and so on. Thus, some models are needed to design the radar reflectors.

* Corresponding author.
E-mail addresses: gildas.kubicke@univ-nantes.fr (G. Kubické), christophe.bourlier@univ-nantes.fr (C. Bourlier), joseph.saillard@univ-nantes.fr (J. Saillard).

1631-0705/$ – see front matter
doi:10.1016/j.crhy.2009.12.001

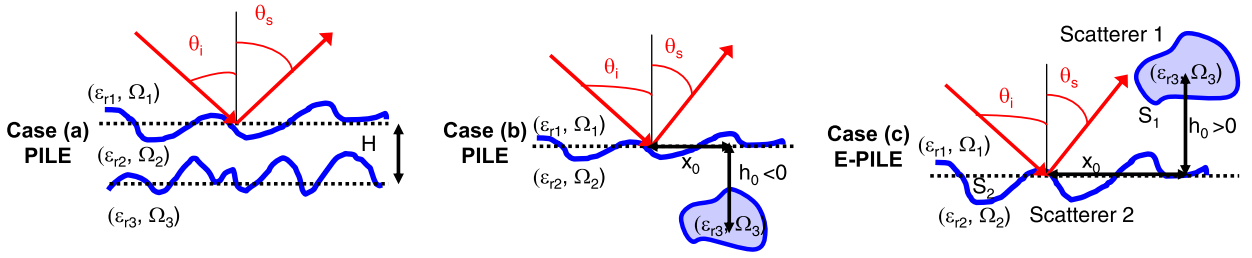

Fig. 1. Description of the problem. (a) Case: scattering by a stack of two rough interfaces separating homogeneous media. (b) Case: scattering by an object *below* a rough surface. Case (c): scattering by an object *above* a rough surface. The media $\{\Omega_1, \Omega_2, \Omega_3\}$ of permittivities $\{\epsilon_{r1}, \epsilon_{r2}, \epsilon_{r3}\}$ are assumed to be homogeneous, and the scatterers are invariant along the direction normal to the figure.

On a related subject, several asymptotic and exact models have been developed for scattering from an object below a rough surface [1–6] and on a rough surface (the object is partially buried) [7,8]. Recently, several studies have led to some asymptotic and exact numerical models for scattering from an object above a rough surface [9,10,3,11] (and references therein). But, in numerical simulations, the surface length plays an important role since a tapered wave is employed to eliminate the finite surface length edge effects [12,13]. So, it is interesting and necessary to investigate exact fast numerical methods to treat such a large problem.

On the one hand, some exact fast numerical methods have been developed for a single rough surface (without the object). For instance, one can quote the Banded-Matrix-Iterative-Approach/CAnonical Grid (BMIA-CAG) of Tsang et al. [14,15] of complexity $\mathcal{O}(N_2 \log N_2)$, the Method of Ordered Multiple Interactions (MOMI) of Kapp et al. [16] of complexity $\mathcal{O}(N_2^2)$, the Forward–Backward (FB) method of Holliday et al. [17] of complexity $\mathcal{O}(N_2^2)$, and the accelerated version Forward-Backward Spectral Acceleration (FB-SA) of Chou et al. [18] of complexity $\mathcal{O}(N_2)$, in which N_2 is the number of unknowns on the rough surface.

On the other hand, Déchamps et al. [19] have recently developed a fast numerical method, PILE (Propagation-Inside-Layer Expansion), devoted to scattering by a stack of two one-dimensional interfaces separating homogeneous media which corresponds to the problem depicted in Fig. 1(a). The main advantage of the PILE method is that the resolution of the linear system (obtained from the Method of Moments: MoM) is broken up into different steps. Two steps are dedicated to solving for the local interactions, which can be done from efficient methods valid for a single rough interface, such FB-SA and BMIA/CAG, and two are dedicated to solving for the coupling interactions.

More recently, the PILE method has been applied by Bourlier et al. [21] to the problem depicted in Fig. 1(b). Kubické et al. [22] have proposed the extended version of the PILE method, called E-PILE (Extended-PILE), in order to treat the more general case of two illuminated surfaces like the case depicted in Fig. 1(c). In addition, to accelerate this method and to treat a large problem, the local interactions on the rough surface are computed from FB-SA. Since the number of unknowns on the rough surface is much greater than that on the object, the complexity of the method is then $\mathcal{O}(N_2)$. For a bistatic configuration, the development of the E-PILE method combined with FB-SA (E-PILE + FB-SA) and its convergence was already described in details in [25], in which scattering from canonical objects above a multi-scale sea surface obeying the Elfouhaily et al. height spectrum [23] was considered.

In this article, the monostatic case is thoroughly investigated. For this configuration, a longer surface (due to the incident beam) and a high computing time are required. Thus, to our knowledge, there is no result of such a complex problem for a monostatic configuration from a rigorous approach. By using the E-PILE + FB-SA method, monostatic results can be obtained for realistic maritime scenes made up of an object (cylinder and cross are considered) above a sea surface. This permits us to confirm, with a rigorous method, some intuitively known conclusions and, also, to establish some new remarks about the monostatic configuration.

The article is organized as follows. In Section 2, a brief summary of the E-PILE + FB-SA method is given and its convergence is tested for a monostatic configuration in Section 3. In Section 4, the algorithm is applied to compute the Normalized Radar Cross-Section (NRCS) of an object (cylinder and cross are considered) located above a sea-like surface at microwave frequencies from a Monte Carlo process. In addition, comparisons are done with results obtained by considering a single rough surface (without the object), the object only (without the sea surface) and the object above a flat surface.

2. The E-PILE method combined with FB-SA

2.1. A rigorous numerical method for the scattering from two scatterers

Let us consider two scatterers (with homogeneous media) embedded in a homogeneous medium as depicted in Fig. 1(c). The use of the integral equations discretized by the MoM leads to the linear system $\bar{\mathbf{Z}}\mathbf{X} = \mathbf{b}$, in which $\bar{\mathbf{Z}}$ is the impedance matrix of the scene made up of the two scatterers, $\mathbf{b}$ the incident field, and $\mathbf{X}$ the current on both the scatterers (the field and its normal derivative on the surfaces). The E-PILE method was developed in order to solve such a linear system

efficiently and rigorously. Indeed, by inverting by block the impedance matrix and using the way of [19,22], it can be shown after some mathematical manipulations that the current $\mathbf{X}_1$ on the surface S_1 of the scatterer 1 is:

$$\mathbf{X}_1 = \sum_{p=0}^{p=P_{\mathrm{PILE}}} \mathbf{Y}_1^{(p)} \tag{1}$$

in which

$$\begin{cases} \mathbf{Y}_1^{(0)} = \bar{\mathbf{Z}}_1^{-1}(\mathbf{b}_1 - \bar{\mathbf{Z}}_{21}\bar{\mathbf{Z}}_2^{-1}\mathbf{b}_2) & \text{for } p = 0 \\ \mathbf{Y}_1^{(p)} = \bar{\mathbf{M}}_{c,1}\mathbf{Y}_1^{(p-1)} & \text{for } p > 0 \end{cases} \tag{2}$$

$\bar{\mathbf{M}}_{c,1}$ being the characteristic matrix of the scene (the two scatterers) defined as $\bar{\mathbf{M}}_{c,1} = \bar{\mathbf{Z}}_1^{-1}\bar{\mathbf{Z}}_{21}\bar{\mathbf{Z}}_2^{-1}\bar{\mathbf{Z}}_{12}$ and $\mathbf{b}_1$ the incident field illuminating the scatterer 1. $\bar{\mathbf{Z}}_1$ and $\bar{\mathbf{Z}}_2$ are the impedance matrices of scatterer 1 and scatterer 2, respectively, whereas $\bar{\mathbf{Z}}_{12}$ and $\bar{\mathbf{Z}}_{21}$ can be interpreted as coupling matrices between the two scatterers. The mathematical expressions of these matrices can be found in [19,21,22]. In Eq. (1), the sum is truncated at order P_{PILE} obtained from a convergence criterion. By substituting subscripts $\{1, 2, 12, 21\}$ for subscripts $\{2, 1, 21, 12\}$ in Eqs. (1) and (2), the unknowns on the surface S_2, $\mathbf{X}_2$, can be found.

$\bar{\mathbf{Z}}_1^{-1}$ accounts for the local interactions on the surface S_1, so $\mathbf{Y}_1^{(0)}$ (zeroth order term) corresponds to the current on the surface of scatterer 1 when it is illuminated by the direct incident field ($\mathbf{b}_1$) and the direct scattered field by the surface S_2 ($-\bar{\mathbf{Z}}_{21}\bar{\mathbf{Z}}_2^{-1}\mathbf{b}_2$). Indeed, $\bar{\mathbf{Z}}_2^{-1}$ accounts for the local interactions on the lower surface, and $\bar{\mathbf{Z}}_{21}$ propagates the field on the surface S_2 toward scatterer 1. In the first-order term, $\mathbf{Y}_1^{(1)} = \bar{\mathbf{M}}_{c,1}\mathbf{Y}_1^{(0)}$, $\bar{\mathbf{Z}}_{12}$ propagates the current on the surface S_1, $\mathbf{Y}_1^{(0)}$, toward scatterer 2, $\bar{\mathbf{Z}}_2^{-1}$ accounts for the local interactions on S_2, and $\bar{\mathbf{Z}}_{21}$ re-propagates the resulting contribution toward scatterer 1; finally, $\bar{\mathbf{Z}}_1^{-1}$ updates the current values on S_1. Thus the characteristic matrix $\bar{\mathbf{M}}_{c,1}$ propagates the field between the two scatterers in a back and forth manner. In conclusion, the order P_{PILE} of E-PILE method, corresponds to the number of back and forths between the scatterers.

Moreover, one of the advantages of the E-PILE method is that the resolution of the linear system $\bar{\mathbf{Z}}\mathbf{X} = \mathbf{b}$ is reduced to an iterative scheme which involves the inverses of the impedance matrix of each surface. Consequently, if one of the scatterers is a rough surface (as in the cases depicted in Fig. 1), the computation of the local interactions on this surface (inversion of $\bar{\mathbf{Z}}_2$ and computation of the matrix–vector product $\bar{\mathbf{Z}}_2^{-1}\mathbf{u}$, where $\mathbf{u}$ is a vector) can be done by using a fast numerical method that already exists for scattering from a single rough surface (without the object). So, the FB-SA method [18] can be used to accelerate the E-PILE method.

2.2. Acceleration of E-PILE by using the FB-SA

The FB-SA method [18] is based on the FB method [17] in which the local interactions are split into forward and backward contributions leading to an iterative procedure. With the Spectral Acceleration, the local interactions (forward and backward contributions) are split into strong and weak interactions. The strong ones are computed exactly, whereas the weak ones are computed approximately by using a spectral decomposition of the Green's function. The key parameters of the FB-SA are then the order P_{FB} involved in the iterative scheme of the FB and the strong interaction length (horizontal distance separating the weak interactions from the strong ones) x_{d0} involved in the SA. For more details, see [17,18,20,21].

For a monostatic configuration (at the scattering angle $\theta_s = -\theta_i$), the field scattered from the scene (object above a rough surface) in far-field region (at a distance r'), $\psi_s(\theta_i)$, is computed by using the Huygens principle; the fields and their normal derivatives on the surfaces (object and sea surface) are obtained from E-PILE + FB-SA. Then, the Normalized Radar Cross Section (NRCS) of the scene is expressed from [12]

$$\sigma(\theta_i) = \frac{r'|\psi_s(\theta_i)|^2}{2\eta_0 P_i} \quad \text{with } P_i = \frac{\cos\theta_i}{2\eta_0} g\sqrt{\frac{\pi}{2}}\left[1 - \frac{1 + 2\tan^2\theta_i}{2k^2g^2\cos^2\theta_i}\right] \tag{3}$$

in which r' is the distance separating the scene from the receiver, $\eta_0 = 120\pi$, g is the Thorsos wave parameter which defines the width of the incident beam. $g = L_2/6$ is a common value. P_i is the Thorsos incident power on the mid-plane of the rough surface [12] which depends on θ_i. This normalization makes the RCS independent of P_i, and so, independent of θ_i and of the surface length L_2.

As seen before, one of the advantages of the E-PILE method is to separate the local interactions of the rough surface and those of the object. Thus, a means to obtain the parameters P_{FB} and x_{d0} is to study the scattering from a *single* rough surface (without the object). A main conclusion drawn in [25] is that the FB-SA method is particularly interesting for maritime applications. Indeed, a convergence study of the FB-SA showed that for a sea surface $x_{d0} = 0.02L_c$ in which the correlation length (corresponding to the gravity waves) is $L_c = 0.154u_{10}^{2.04}$ for a sea-like surface [24] whereas for a Gaussian spectrum $x_{d0} = 3L_c$. In the following, by considering the results obtained in [25], an order $P_{\mathrm{FB}} = \{5, 2\}$ for {H, V polarization} and a ratio $\alpha = 0.05$ ($x_{d0} = 0.05L_c$) are chosen in order to insure the good convergence of FB-SA, whatever the considered scene. For example, with this ratio, the strong interaction length is only $x_{d0} = 0.2$ m with $u_{10} = 5$ m/s.

Table 1
RRE versus the order P_{PILE} for the H polarization and for two canonical objects above a rough surface. $f = 3$ GHz, $\epsilon_r = 70.4 + 40.6i$, $u_{10} = 5\ \mathrm{m\,s^{-1}}$, sampling step $\lambda_0/10$, $N_2 = 4000$ samples and Thorsos wave parameter $g = L_2/6$.

Object	P_{PILE}					
	0	1	2	3	4	5
Cylinder	0.2792	0.0322	0.0142	0.0063	0.0032	0.0028
Cross	0.3347	0.1139	0.0558	0.0279	0.0110	0.0047

3. Convergence of E-PILE + FB-SA

In this section, for a monostatic configuration, the convergence of E-PILE + FB-SA is studied for the scattering from perfectly-conducting canonical objects above a rough sea surface. As seen in Section 2, the E-PILE method is applied and accelerated by using FB-SA for the local interactions on the rough surface. Two scenes are considered: a circular cylinder above a sea surface and a cross above a sea surface.

For each scene, $f = 3$ GHz, $\epsilon_r = 70.4 + 40.6i$, $u_{10} = 5$ m/s, $L_2 = 400\lambda_0 = 40$ m, $\Delta_{x_2} = \lambda_0/10$ ($N_2 = 4000$), $g = L_2/6$. H polarization is considered. We set $P_{\mathrm{FB}} = 5$ and $\alpha = 0.05$ ($x_{d0} = 0.2$ m). The circular cylinder has a radius $a = 5\lambda_0 = 0.50$ m and is described by $N_1 = 314$ samples. The cross is made up of four plates with $L_1 = 5\lambda_0 = 0.5$ m; it is described by $N_1 = 400$ samples and oriented in such a manner that two plates are oriented horizontally and the other two are oriented vertically. Consequently, these two canonical objects are circumscribed in a circle with a diameter $D = 1$ m. The center of each object is located at ($x_0 = -h_0 \tan(\theta_i)$, $h_0 = 30\lambda_0 = 3$ m) in such a way that each object is centered on the Thorsos wave for any incidence angle. One surface realization is considered. To stop the algorithm at order P_{PILE}, a criterion is defined by a Relative Residual Error (RRE) smaller than a threshold chosen equal to 10^{-2}, where the RRE is given by

$$\mathrm{RRE} = \frac{\mathrm{norm}(\boldsymbol{\sigma} - \boldsymbol{\sigma}_{\mathrm{LU}})}{\mathrm{norm}(\boldsymbol{\sigma}_{\mathrm{LU}})} \tag{4}$$

in which "norm" corresponds to the Euclidean norm of a vector, $\boldsymbol{\sigma}$ and $\boldsymbol{\sigma}_{\mathrm{LU}}$ are the vectors which contain the NRCS versus the scattering angle obtained from the method under test (E-PILE + FB-SA) and the classic MoM (with direct LU inversion: MoM + LU), respectively.

Table 1 presents the RRE obtained from E-PILE + FB-SA for the two scenes and versus the order P_{PILE}.

From Table 1, as the order P_{PILE} increases, the RRE decreases. Indeed, the order P_{PILE} corresponds to the number of back and forths between the object and the sea surface, so the coupling is better taken into account with a high order P_{PILE}. E-PILE + FB-SA converges (under the criterion RRE $< 10^{-2}$) for the cylinder from $P_{\mathrm{PILE}} = 3$ and from $P_{\mathrm{PILE}} = 5$ for the cross above the sea surface. Thus, the convergence is obtained very rapidly. Same results are obtained in V polarization and for other frequencies.

In Figs. 2(a) and 2(b), the NRCS for the circular cylinder and the cross above the sea surface are depicted respectively. For each figure, the E-PILE + FB-SA method is compared with MoM + LU (with direct LU inversion). The same parameters as in Table 1 are considered.

From Figs. 2(a) and 2(b), very good agreement between E-PILE + FB-SA and MoM + LU is observed. Consequently, the E-PILE + FB-SA method can be used to study rigorously a more realistic scene which implies a high number of unknowns.

4. Monte Carlo simulations for an object above a sea-like rough surface for the monostatic case

4.1. Criterion for the convergence of E-PILE + FB-SA

For more realistic results, the random behavior of the scene must be taken into account. This is done with the Monte Carlo process. By using a spectral method, several independent surfaces (but with the same Gaussian process and the same height spectrum) are generated. A cross is put above each generated surface at the same position (x_0, h_0). For each scene (numbered "r") the scattered field ψ_r is calculated from E-PILE + FB-SA at order P_{PILE} and versus the incident angle θ_i. Then, the NRCS (total component: uncentered second-order moment) with the Monte Carlo process is evaluated from

$$\sigma(\theta_i, P_{\mathrm{PILE}}) = \frac{r' \langle |\Psi_{P_{\mathrm{PILE}}}(\theta_i)|^2 \rangle}{2\eta_0 P_i} \tag{5}$$

with

$$\left\langle \left|\Psi_{P_{\mathrm{PILE}}}(\theta_i)\right|^2 \right\rangle = \frac{1}{R} \sum_{r=1}^{r=R} \left|\psi_r(\theta_i, P_{\mathrm{PILE}})\right|^2 \tag{6}$$

As seen previously, the higher the order P_{PILE}, the more the method E-PILE + FB-SA converges to the MoM + LU. A criterion is used to choose the order P_{PILE} which provides a good convergence (called P_{conv}). The NRCS is evaluated with E-PILE + FB-SA for $P_{\mathrm{PILE}} = \{1, 2, \ldots, P_{\max}\}$. P_{conv} is obtained with the following criterion (with $\theta_i \in [0; 70]^\circ$):

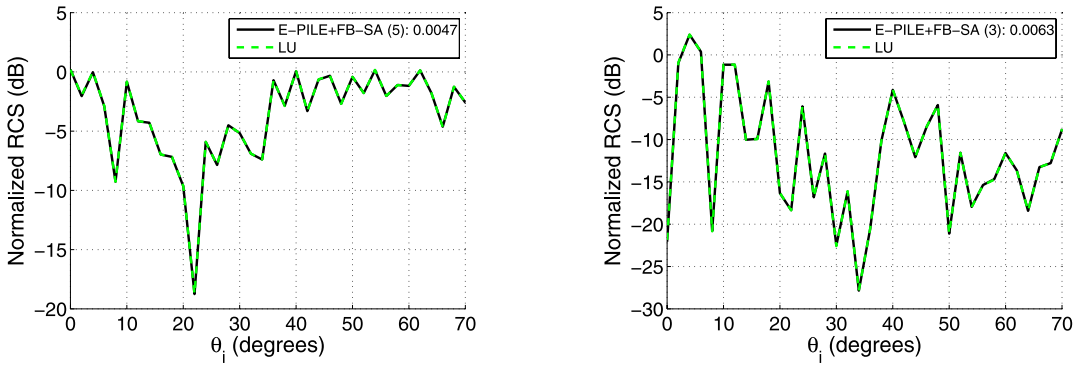

(a) Cross above a rough sea surface

(b) Cylinder above a rough sea surface

Fig. 2. Comparison of the NRCS of an object above a sea surface computed from E-PILE + FB-SA with the one computed from a direct LU inversion versus the incidence angle. The radius of the cylinder is $a = 5\lambda_0 = 0.5$ m, $N_1 = 314$. For the cross, each plate has a length $L_1 = 0.5$ m ($N_1 = 400$). The object is located at ($x_0 = -h_0 \tan(\theta_i)$, $h_0 = 3$ m) and same parameters as in Table 1. In the legend, the order P_{PILE} in parenthesis and the RRE.

$$P_{\text{conv}} = \left\{ (P_{\text{PILE}} + 1) / \max\left(\left| \sigma_{\text{dB}}(\theta_i, P_{\text{PILE}} + 1) - \sigma_{\text{dB}}(\theta_i, P_{\text{PILE}}) \right| \right) < S_0 \right\} \tag{7}$$

in which $\max(\mathbf{x})$ provides the maximum value of the vector $\mathbf{x}$ over θ_i, σ_{dB} represents the NRCS σ expressed in dB and S_0 is a threshold expressed in dB. In this paper, we set $S_0 = 0.1$ dB.

4.2. Numerical results

For a monostatic configuration, numerical results of the NRCS (given by Eq. (5)) are presented for a perfectly-conducting object (cylinder and cross) located above a rough sea surface by considering 50 realizations ($R = 50$). Comparisons are done with the results obtained by considering the sea surface only (without the object), the object only (without the sea) and the object above a flat surface. For all the results presented here: the frequency is $f = 5.3$ GHz, the relative permittivity of the sea surface is $\epsilon_r = 69 + 35i$, $L_2 = 80$ m, $\Delta_{x_2} = \lambda_0/8$ ($N_2 = 11\,307$), $g = L_2/6$. The cross is described by $N_1 = 560$ samples, with $L_1 = 0.5$ m, centered on ($x_0 = -h_0 \tan(\theta_i)$, $h_0 = 3$ m). The cylinder is described by $N_1 = 440$ samples, with $a = 0.5$ m, centered on ($x_0 = -h_0 \tan(\theta_i)$, $h_0 = 3$ m).

The NRCS of the cross above the sea surface in H polarization with $u_{10} = 5$ m/s and $u_{10} = 10$ m/s are plotted in Figs. 3(a) and 3(b), respectively. The NRCS of the cross above the sea surface in V polarization with $u_{10} = 5$ m/s and $u_{10} = 10$ m/s are plotted in Figs. 4(a) and 4(b), respectively.

The NRCS of the cylinder above the sea surface in H polarization with $u_{10} = 5$ m/s and $u_{10} = 10$ m/s are plotted in Figs. 5(a) and 5(b), respectively. The NRCS of the cylinder above the sea surface in V polarization with $u_{10} = 5$ m/s and $u_{10} = 10$ m/s are plotted in Figs. 6(a) and 6(b), respectively.

The convergence of E-PILE + FB-SA under the criterion given in Eq. (7) is reached with $P_{\text{conv}} = 2$ for results obtained in Figs. 3(a), 3(b), 4(a), 4(b) and 6(b) and reached with $P_{\text{conv}} = 3$ for results obtained in Figs. 5(a), 5(b) and 6(a). Thus, E-PILE + FB-SA converged in only few iterations. From these results, one can notice that for $\theta_i < 15°$, the NRCS of the object above the sea surface is very close to that obtained with the sea surface only. Indeed, for low incidence angles, the backscattering direction is close to the specular direction; thus, the object response is drowned out by the strong contribution of the sea surface only, except for $\theta_i = 0°$ which is due to specular single reflections of the two horizontal plates of the cross. The specular reflection of the cylinder is very lower than that of the cross and, so, its contribution is not perceptible at $\theta_i = 0°$. From $\theta_i > 15°$, the more the backscattering direction departs from the specular direction, the more the contribution of the sea surface only decreases. The object effect (direct reflection and coupling) is more important.

From Figs. 3(a) to 6(b), one can notice that from $\theta_i > 15°$, the cross above the sea surface provides a stronger monostatic NRCS than that obtained with the cylinder above the sea surface. Same observations can be made by considering the results obtained with the objects above the flat surface. This is physically due to the object shape: the cross facilitates intrinsically the return of the incident wave by means of double reflections between the faces whereas the cylinder spread the energy over a wide angular range. This can be seen with results obtained with the object only (without the sea surface). The object shape plays an important role in the NRCS of the scene.

One can notice that the NRCS of the cylinder in free space depends on θ_i. Indeed, this does not correspond to the RCS of the cylinder since there is a normalization by P_i which depends on θ_i (see Eq. (3)). For the cross case, for $\theta_i \in [25°; 60°]$ for H polarization and for $\theta_i \in [25°; 70°]$ for V polarization, the NRCS of the cross above the sea equals the NRCS of the cross in free space. This could mean that there is no coupling between the cross and the sea. For the cylinder case, the difference of the NRCS of the cylinder above the sea and that obtained with the cylinder in free space indicates that there is a strong coupling between the cylinder and the sea.

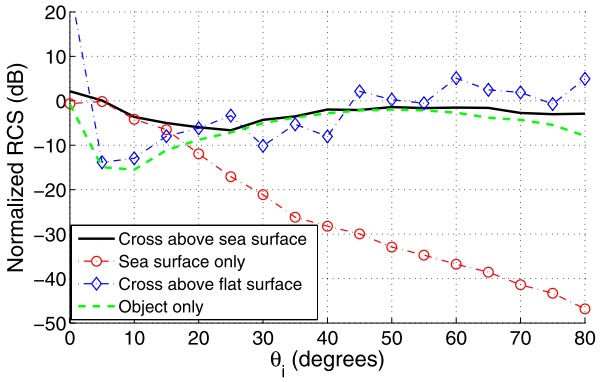

(a) H polarization, $u_{10} = 5$ m/s

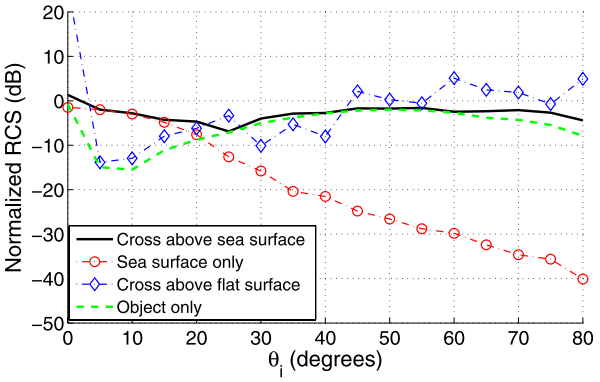

(b) H polarization, $u_{10} = 10$ m/s

Fig. 3. Normalized Radar Cross Section of a cross above a rough sea surface.

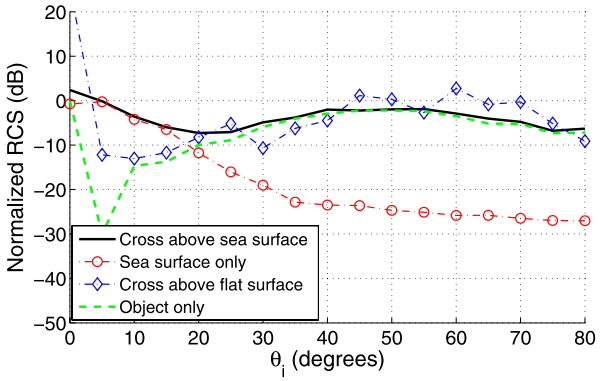

(a) V polarization, $u_{10} = 5$ m/s

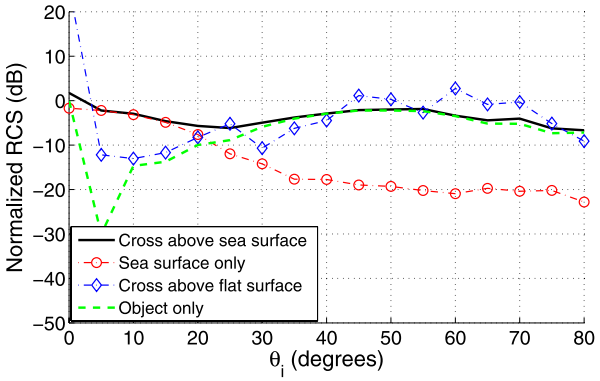

(b) V polarization, $u_{10} = 10$ m/s

Fig. 4. Normalized Radar Cross Section of a cross above a rough sea surface.

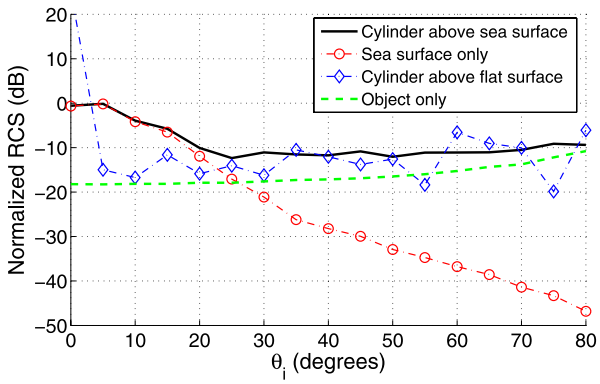

(a) H polarization, $u_{10} = 5$ m/s

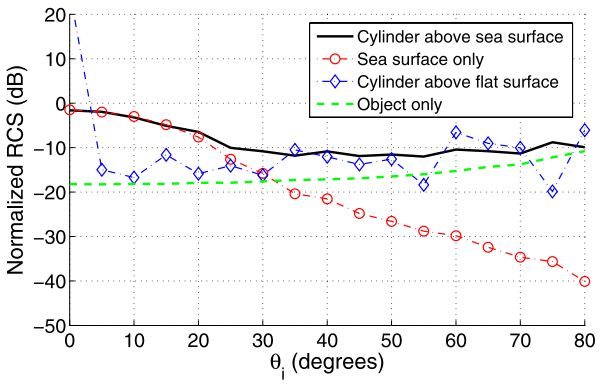

(b) H polarization, $u_{10} = 10$ m/s

Fig. 5. Normalized Radar Cross Section of a cylinder above a rough sea surface.

From $\theta_i > 30°$, the NRCS of the sea surface in V polarization is stronger than in H polarization whereas for an object above the sea surface the NRCS is not very sensitive to the polarization. Indeed, from $\theta_i > 30°$, the object effect (direct reflection and coupling) is more important and the object response are quite similar whatever the polarization.

For an object above a flat surface, an oscillating behavior is observed. It is due to constructive and destructive contributions. For an object above the sea surface, the response is smooth.

In order to better understand the coupling between the object and the sea, the incoherent component (centered second-order moment of the scattered field) and the coherent component (total component minus the incoherent component) of

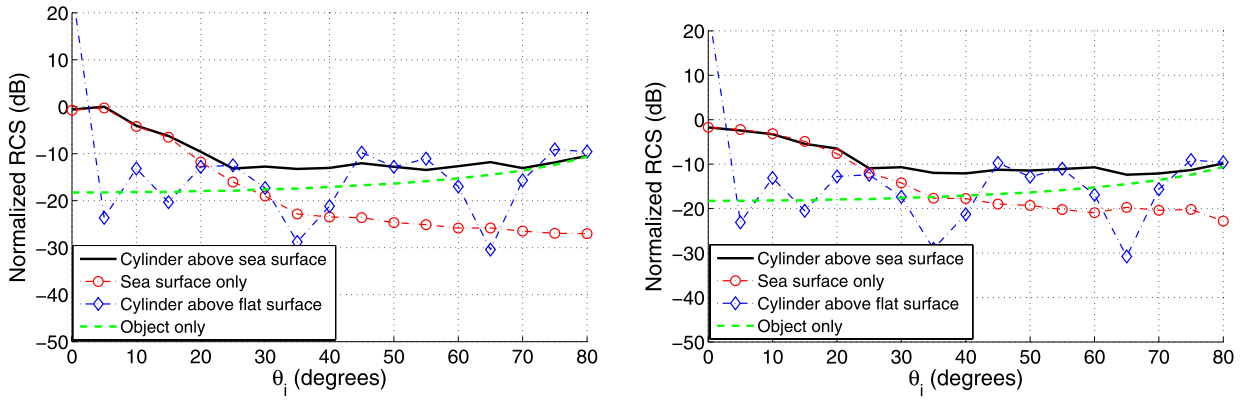

(a) V polarization, $u_{10} = 5$ m/s

(b) V polarization, $u_{10} = 10$ m/s

Fig. 6. Normalized Radar Cross Section of a cylinder above a rough sea surface.

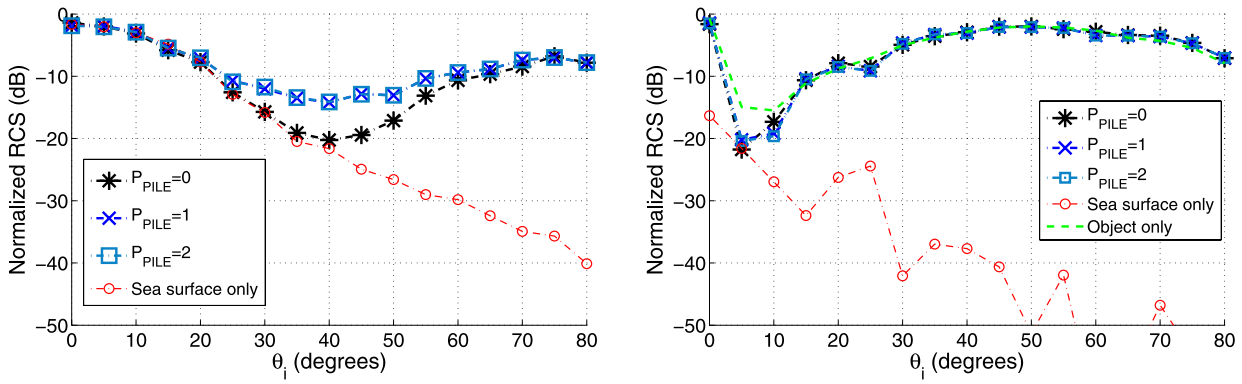

(a) Incoherent components

(b) Coherent components

Fig. 7. Incoherent and coherent components of the NRCS of a cross above a rough sea surface for different values of P_{PILE} for H polarization with $u_{10} = 10$ m/s. In addition, the incoherent and coherent components of the NRCS of sea surface only and the coherent component of the NRCS of the cylinder only are plotted.

the NRCS can be studied. The incoherent component is related to the random behavior of the scene whereas the coherent component is related to the deterministic one. For the cross above the sea surface in H polarization with $u_{10} = 10$ m/s, these two NRCS components are plotted in Figs. 7(a) and 7(b), respectively.

In spite of the fact that the coupling is not really significant in the total component (see Fig. 5(b)) for $\theta_i \in [25°; 60°]$, one can see a strong coupling in the incoherent component (see Fig. 7(a)). Indeed, results with the cross above the sea differ significantly from those with the sea surface only. The cross only does not provide incoherent component. Moreover, in Fig. 7(a), the coupling appears from $\theta_i = 40°$ for $P_{\text{PILE}} = 0$ (only one interaction between the object and the sea). It becomes stronger and appears from $\theta_i = 25°$ as the order P_{PILE} increases (more interaction are considered). Nevertheless, for the coherent component (see Fig. 7(a)), the coupling is significant only for $\theta_i \leqslant 15°$. One can notice that if the cross orientation is modified, the specular directions of single and double reflections will be different. Thus, the coherent component will be strongly modified (angular translation) and then, the total component of the NRCS will be modified. Same conclusions can be drawn with the scenes considered in Figs. 5(a), 6(b) and 6(a).

Comparisons of the total, incoherent and coherent components of the NRCS of the cylinder above a sea surface with $u_{10} = 5$ m/s for H and V polarizations, are plotted in Figs. 8(a) and 8(b), respectively. In addition, the total components of the NRCS of the sea surface only (in free space) and that of the cylinder in free space are plotted.

From Figs. 8(a) and 8(b), unlike the cross case, the total component for the cylinder above the sea is due to both coherent and incoherent components for $\theta_i > 25°$. Moreover, an energy conversion from coherent to incoherent component can be seen: as the incoherent component decreases, the coherent one increases. In spite of the fact that the sea clutter (sea surface only) is higher for V polarization, the incoherent component is higher for H polarization. This explains why quite similar results are obtained for both polarizations. This means that the coupling is stronger for H polarization. Indeed, for this polarization, since the backscattering is lower, most of the energy is spread over bistatic angles, thus, in particular toward the cylinder. The energy is redirected toward the monostatic direction with the help of the cylinder. Once again, for these

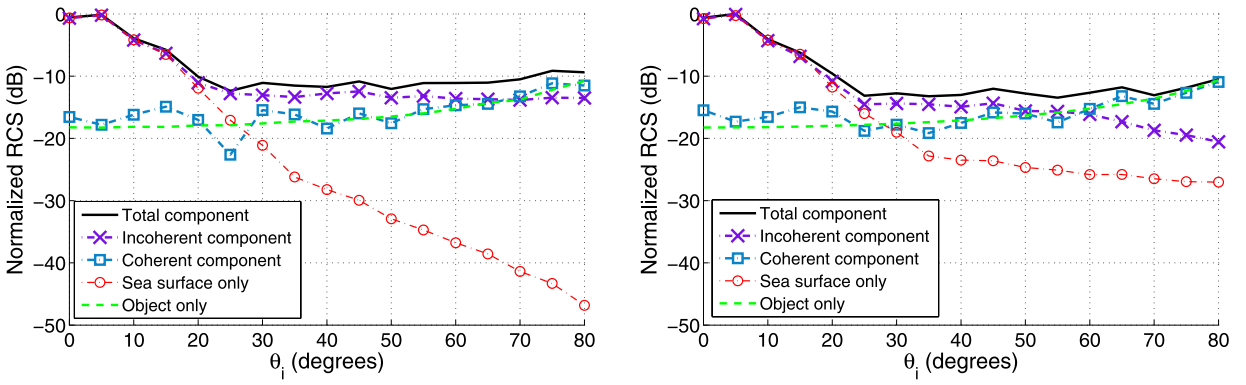

(a) H polarization, $u_{10} = 5$ m/s

(b) V polarization, $u_{10} = 5$ m/s

Fig. 8. Comparisons of the different components of the Normalized Radar Cross Section of a cylinder above a rough sea surface. In addition, the total component of the NRCS of the sea surface only and that of the cylinder only are plotted.

configurations, coupling do not very occur in the coherent component (similar results than those obtained with the cylinder in free space). If the height of the cylinder h_0 is modified, coupling will slightly change, and thus, the total component too.

From this study, one can conclude:

- an object which gives intrinsically a high monostatic RCS in free space (the cross here) makes its detection easier when put above the sea;
- a low sea state ($u_{10} = 5$ m/s) makes the object detection easier when put above the sea. Indeed, the sea clutter is stronger with a higher sea state ($u_{10} = 10$ m/s) which makes the object detection more difficult;
- the roughness effect implies a smoothing of the monostatic RCS. The fading effects, obtained with an object above a flat surface, disappear by considering a rough sea surface;
- since the sea clutter is lower in H polarization than in V polarization, the H polarization makes the object detection easier when put above the sea;
- the coupling is stronger in H polarization;
- only few interactions between the object and the sea are needed to take into account the coupling effect;
- with the parameters considered in this paper, the coupling occurs in the incoherent component.

5. Conclusion

In this article, scattering from canonical objects above a sea-like one-dimensional rough surface in monostatic configuration is investigated. Since such a problem can not be solved easily with a classic Method of Moments (with direct LU inversion), a recently developed fast numerical method called E-PILE is used. This allows us to use the Forward-Backward Spectral Acceleration (FB-SA) for the computation of local interactions on the sea surface which is particularly interesting for a maritime context. Then, the convergence of E-PILE + FB-SA is investigated for scattering from a canonical object (cylinder and cross) located above a sea surface in monostatic configuration. This study leads to an important conclusion: E-PILE + FB-SA can be considered as a benchmark method whatever the shape of the object. Indeed, although the two objects imply different scattering mechanisms, the E-PILE + FB-SA method converges to MoM + LU very rapidly. Since $N_2 \gg N_1$, the complexity of this approach is $\mathcal{O}(N_2)$ which permits to compute the scattering from an object above a very long sea surface. Thus, this method is appropriate for a maritime application at microwave frequencies, for which, the MoM + LU can not be used with a standard personal computer. By using the Monte Carlo process, realistic results obtained from E-PILE + FB-SA method are presented and the physical mechanisms of the coupling between the object and the sea surface have been studied. Thus, one can show that the object detection is easier in H polarization, with a slightly rough sea surface (low sea state), at high incidence angles and when the object shape provides a high monostatic RCS in free space.

Acknowledgement

This work was supported by the French defence procurement agency DGA (Délégation générale pour l'armement) under REI grant 2008.34.0041.

References

[1] A. Madrazo, M. Nieto-Vesperinas, Scattering of light and other electromagnetic waves from a body buried beneath a highly rough random surface, Journal of the Optical Society of America 14 (1997) 1859–1866.

[2] D.E. Lawrence, K. Sarabandi, Electromagnetic scattering from a dielectric cylinder buried beneath a slightly rough surface, IEEE Transactions on Antennas and Propagation 50 (2002) 1368–1376.
[3] X. Wang, C.-F. Wang, Y.-B. Gan, L.-W. Li, Electromagnetic scattering from a circular target above or below rough surface, Progress In Electromagnetics Research 40 (2003) 207–227.
[4] J.T. Johnson, R.J. Burkholder, A study of scattering from an object below a rough surface, IEEE Transactions on Geoscience and Remote Sensing 42 (2004) 59–66.
[5] C.-H. Kuo, M. Moghaddam, Electromagnetic scattering from a buried cylinder in layered media with rough interfaces, IEEE Transactions on Antennas and Propagation 54 (2006) 2392–2401.
[6] Y. Altuncu, A. Yapar, I. Akduman, On the scattering of electromagnetic waves by bodies buried in a half-space with locally rough interface, IEEE Transactions on Geoscience and Remote Sensing 44 (2006) 1435–1443.
[7] M.R. Pino, R. Burkholder, F. Obelleiro, Spectral acceleration of the generalized forward–backward method, IEEE Transactions on Antennas and Propagation 50 (June 2002) 785–797.
[8] Z.-X. Li, Bistatic scattering from rough dielectric soil surface with a conducting object with arbitrary closed contour partially buried by using the FBM/SAA method, Progress In Electromagnetics Research 76 (2007) 253–274.
[9] Y. Zhang, Y.E. Yang, H. Braunisch, J.A. Kong, Electromagnetic wave interaction of conducting object with rough surface by hybrid SPM/MoM technique, Progress In Electromagnetics Research 22 (1999) 315–335.
[10] J.T. Johnson, A numerical study of scattering from an object above a rough surface, IEEE Transactions on Antennas and Propagation. 50 (10) (2002) 1361–1367.
[11] H. Ye , Y.-Q. Jin, A hybrid analytic-numerical algorithm of scattering from an object above a rough surface, IEEE Transactions on Antennas and Propagation 45 (5) (2007) 1174–1180.
[12] L. Tsang, J.A. Kong, K.-H. Ding, C.O. Ao, Scattering of Electromagnetics Waves: Vol. II. Numerical Simulations, Wiley Series on Remote Sensing, Wiley, 2001.
[13] E.I. Thorsos, The validity of the Kirchhoff approximation for rough surface scattering using a Gaussian roughness spectrum, Journal of the Acoustical Society of America 83 (1988) 78–92.
[14] L. Tsang, C.H. Chang, H. Sangani, A banded matrix iterative approach to Monte Carlo simulations of scattering of waves by large scale random rough surface problems: TM case, Electronic Letters 29 (1993) 1666–1667.
[15] L. Tsang, C.H. Chang, H. Sangani, A. Ishimaru, P. Phu, A banded matrix iterative approach to Monte Carlo simulations of large scale random rough surface scattering: TE case, Journal of Electromagnetic Waves and Applications 29 (1993) 1185–1200.
[16] D. Kapp, G. Brown, A new numerical method for rough-surface scattering calculations, IEEE Transactions on Antennas and Propagation 44 (5) (1996) 711–722.
[17] D. Holliday, L.L. DeRaad Jr., G.J. St-Cyr, Forward–backward: a new method for computing low-grazing angle scattering, IEEE Transactions on Antennas and Propagation 44 (5) (1996) 722–729.
[18] H.T. Chou, J.T. Johnson, A novel acceleration algorithm for the computation of scattering from rough surfaces with the forward–backward method, Radio Science 33 (1998) 1277–1287.
[19] N. Déchamps, N. De Beaucoudrey, C. Bourlier, S. Toutain, Fast numerical method for electromagnetic scattering by rough layered interfaces: Propagation-inside-layer expansion method, Journal of the Optical Society of America A 23 (2006) 359–369.
[20] N. Déchamps, C. Bourlier, Electromagnetic scattering from a rough layer: Propagation-inside-layer expansion method combined to the forward–backward novel spectral acceleration, IEEE Transactions on Antennas and Propagation 55 (12) (2007) 33576–33586.
[21] C. Bourlier, G. Kubické, N. Déchamps, A fast method to compute scattering by a buried object under a randomly rough surface: PILE combined with FB-SA, Journal of the Optical Society of America A 25 (April 2008) 891–902.
[22] G. Kubické, C. Bourlier, J. Saillard, Scattering by an object above a randomly rough surface from a fast numerical method: extended PILE method combined with FB-SA, Waves in Random and Complex Media 18 (August 2008) 495–519.
[23] T. Elfouhaily, B. Chapron, K. Katsaros, D. Vandermark, A unified directional spectrum for long and short wind-driven waves, Journal of Geophysical Research 102 (C7) (1997) 781–796.
[24] C. Bourlier, G. Berginc, Microwave analytical backscattering models from randomly rough anisotropic sea surface – comparison with experimental data in C and Ku bands, Progress Electromagnetics Research 37 (2002) 31–78.
[25] G. Kubické, C. Bourlier, J. Saillard, Scattering from canonical objects above a sea-like 1D rough surface from a rigorous fast method, Waves in Random and Complex Media (2010), in press.